Bulletin of the Seismological Society of America, Vol. 97, No. 5, pp. 1511–1524, October 2007, doi: 10.1785/0120070007

Beyond Sa_{GMRotI}: Conversion to Sa_{Arb}, Sa_{SN}, and Sa_{MaxRot}

by Jennie A. Watson-Lamprey and David M. Boore

Abstract In the seismic design of structures, estimates of design forces are usually provided to the engineer in the form of elastic response spectra. Predictive equations for elastic response spectra are derived from empirical recordings of ground motion. The geometric mean of the two orthogonal horizontal components of motion is often used as the response value in these predictive equations, although it is not necessarily the most relevant estimate of forces within the structure. For some applications it is desirable to estimate the response value on a randomly chosen single component of ground motion, and in other applications the maximum response in a single direction is required. We give adjustment factors that allow converting the predictions of geometric-mean ground-motion predictions into either of these other two measures of seismic ground-motion intensity. In addition, we investigate the relation of the strike-normal component of ground motion to the maximum response values. We show that the strike-normal component of ground motion seldom corresponds to the maximum horizontal-component response value (in particular, at distances greater than about 3 km from faults), and that focusing on this case in exclusion of others can result in the underestimation of the maximum component. This research provides estimates of the maximum response value of a single component for all cases, not just near-fault strike-normal components. We provide modification factors that can be used to convert predictions of ground motions in terms of the geometric mean to the maximum spectral acceleration (Sa_{MaxRot}) and the random component of spectral acceleration (Sa_{Arb}). Included are modification factors for both the mean and the aleatory standard deviation of the logarithm of the motions.

Introduction

Boore *et al.* (2006) defined an orientation-independent method for computing the geometric mean of spectral accelerations (*Sa*) recorded in two orthogonal horizontal directions. This quantity, referred to here as Sa_{GMRotI}, corresponds to the median geometric-mean response spectra of the two as-recorded horizontal components after a single period-independent rotation that minimizes the variation away from the median value over all useable periods. Sa_{GMRotI} has been chosen as the dependent variable in updating the ground-motion prediction equations (GrMPEs) of Abrahamson and Silva (1997), Boore *et al.* (1997), Campbell and Bozorgnia (2003a, b, c, 2004), and Sadigh *et al.* (1997), as part of a multiyear project sponsored by the Pacific Earthquake Engineering Research Center (PEER Next Generation Attenuation [NGA] Project, http://peer.berkeley.edu/lifelines/repngamodels.html). The previous versions of the updated GrMPEs used the geometric-mean response spectra of the two as-recorded horizontal components (Sa_{GMAR}). In engineering applications, however, some other measure of seismic intensity may be desired (e.g., Baker and Cornell, 2006). Many such measures are listed by Beyer and Bommer (2006), who provide conversion factors between the various measures, for both the medians and the standard deviations. Our article is similar to that of Beyer and Bommer (2006), but with a more restricted scope: we present conversion factors from Sa_{GMRotI} to the spectral acceleration of a randomly chosen component of motion (Sa_{Arb}, where "Arb" stands for "Arbitrary") and to the maximum possible spectral acceleration over all possible orientations of a horizontal component of ground motion (Sa_{MaxRot}). Another measure of the maximum spectral acceleration would be the maximum of the two spectral accelerations from a randomly oriented pair of orthogonal motions; we denote this as Sa_{MaxArb}, and conversion factors to this from Sa_{GMRotI} are given by Beyer and Bommer (2006) and by Campbell and Bozorgnia (2006). We discuss the spectral acceleration in the strike-normal direction (Sa_{SN}; also known as "fault-normal"), but because we find that it rarely corresponds to Sa_{MaxRot}, we do not give any conversion factors for Sa_{SN}.

Our study also differs from that of Beyer and Bommer (2006) in our choice of the subset of the PEER NGA database, as well as in our providing equations for the conversion factor $\ln(Sa_{\mathrm{MaxRot}}/Sa_{\mathrm{GMRotI}})$ as a function of magnitude, distance, and a simplified radiation pattern. We find that the

sensitivity to these variables is small, and that the Beyer and Bommer conversion factors are in reasonably good agreement with our factors. We also find that the ratio $Sa_{\mathrm{MaxRot}}/Sa_{\mathrm{GMRotI}}$ is insensitive to the most commonly used directivity factor; this is not to say that either Sa_{MaxRot} or Sa_{GMRotI} is insensitive to directivity, but only that any sensitivity must be similar for both quantities. Watson-Lamprey (2007) and Spudich and Chiou (2006) found that Sa_{GMRotI} is dependent on directivity factors for pseudospectral acceleration at periods greater than or equal to 3 sec.

Because the predictions of seismic ground-motion intensity Y given by GrMPEs are in terms of the mean of ln Y and the standard deviation $\sigma_{\ln Y}$, we present conversion factors for these two quantities. For example, we convert from the distribution of Y_1 to the distribution of Y_2 by using these equations:

$$E[\ln Y_2] = E[\ln Y_1] + E[\ln(Y_2/Y_1)] \quad (1)$$

and

$$\sigma^2_{\ln Y_2} = \sigma^2_{\ln Y_1} + \sigma^2_{\ln(Y_2/Y_1)} + 2r_{Y_1,Y_2/Y_1}\sigma_{\ln Y_1}\sigma_{\ln(Y_2/Y_1)} \quad (2)$$

where $r_{Y_1,Y_2/Y_1}$ is the correlation coefficient of ln Y_1 and ln(Y_2/Y_1). In this article we give the conversion factors $E(\ln(Y_2/Y_1))$, $\sigma_{\ln(Y_2/Y_1)}$, and $r_{Y_1,Y_2/Y_1}$.

For our analysis we use the PEER NGA database (http://peer.berkeley_edu/nga). The database consists of 7080 individual horizontal-component acceleration time series from 175 earthquakes (there are 3529 two-horizontal-component records and 22 records with only one horizontal component). The subset used in this study includes all two-horizontal-component records with finite fault data, 3397 pairs. Unless noted otherwise we used the complete dataset, subject to the restriction that we only use spectra for periods less than the maximum useable period, as given in the PEER NGA database.

Sa_{Arb}

We know from Boore *et al.* (2006) that the median values of the as-recorded geometric mean and the orientation-independent geometric mean are very similar and that their probability distribution function (PDF) is well represented by a longnormal distribution. In addition, because of the definition of the geometric mean we have:

$$\ln Sa_{\mathrm{GMAR}} = 0.5 \ln Sa_x + 0.5 \ln Sa_y \quad (3)$$

where Sa_{GMAR} is the geometric mean of the spectral accelerations Sa_x and Sa_y in two orthogonal as-recorded directions. The expected value of ln Sa_{GMAR} is given by:

$$E(\ln Sa_{\mathrm{GMAR}}) = 0.5E(\ln Sa_x) + 0.5E(\ln Sa_y). \quad (4)$$

Because Sa_x and Sa_y are randomly chosen, their expected values are equal and are also equal to the expected value of Sa_{Arb}. Thus we have:

$$E(\ln Sa_{\mathrm{GMAR}}) = E(\ln Sa_{\mathrm{Arb}}) \quad (5)$$

so the only adjustment needed for Sa_{Arb} is to multiply Sa_{GMRotI} by the ratio $Sa_{\mathrm{GMAR}}/Sa_{\mathrm{GMRotI}}$. This ratio is near unity, varying from about 0.99 for $T = 0.02$ sec to 0.98 for $T = 3$ sec (see Fig. 10 in Boore *et al.*, 2006). Adjustments to the standard deviation of the PDF are more important. From the preceding analysis, we expect Sa_{Arb} to be lognormally distributed. The standard deviation of the PDF can be estimated from this equation:

$$\sigma^2_{\ln Sa_{\mathrm{Arb}}} = \sigma^2_{\ln Sa_{\mathrm{GMRotI}}} + \sigma^2_C \quad (6)$$

where σ_C is due to component-to-component variation of amplitude, as given by equation (6) of Boore (2005). There should be another contribution due to the uncertainty in the ratio $Sa_{\mathrm{GMAR}}/Sa_{\mathrm{GMRotI}}$, but based on Figure 10 in Boore *et al.* (2006), we expect this to be small and choose to ignore it. We have used the equation in Boore (2005) to calculate σ_C for the subset of the NGA dataset used by Boore and Atkinson (2006) in developing their GrMPEs. The results are given in Table 1. Also shown in the table are the values of σ_C obtained by Beyer and Bommer (2006) and Campbell and Bozorgnia (2006), using different subsets of the NGA database. In general, the values are similar. The last column in the table contains the average values of the first three columns; we suggest that this column be used in computing $\sigma_{\ln Sa_{\mathrm{Arb}}}$.

Sa_{SN}

The prevailing model for predicting directivity amplification is currently the model developed by Somerville *et al.* (1997). It assumes that directivity results from constructive interference of *SH* waves propagating just ahead of the rupture front. To quantify directivity, Somerville *et al.* (1997) developed period-dependent scaling factors for 5%-damped horizontal *Sa* at vibration periods between 0.5 and 5.0 sec. Their model consists of two modifications that apply to median predictions of horizontal *Sa* from spectral attenuation formulas (Somerville *et al.*, 1997). The first of these modifications yields the directivity-amplified average horizontal component, Sa_{Dir}, and the second modification resolves Sa_{Dir} into strike-normal (SN) and strike-parallel (SP) components, Sa_{SN} and Sa_{SP}. (We use "strike-normal" and "strike-parallel" rather than the more commonly used "fault-normal" and "fault-parallel" for two reasons: [1] they are the terms used by Somerville *et al.* [1997]; [2] for faults dipping at an angle of less than 90° the true fault-normal motion would have a vertical component, whereas only the horizontal component is of concern to us in this article—it is understood that the normal to the strike is in the horizontal plane.)

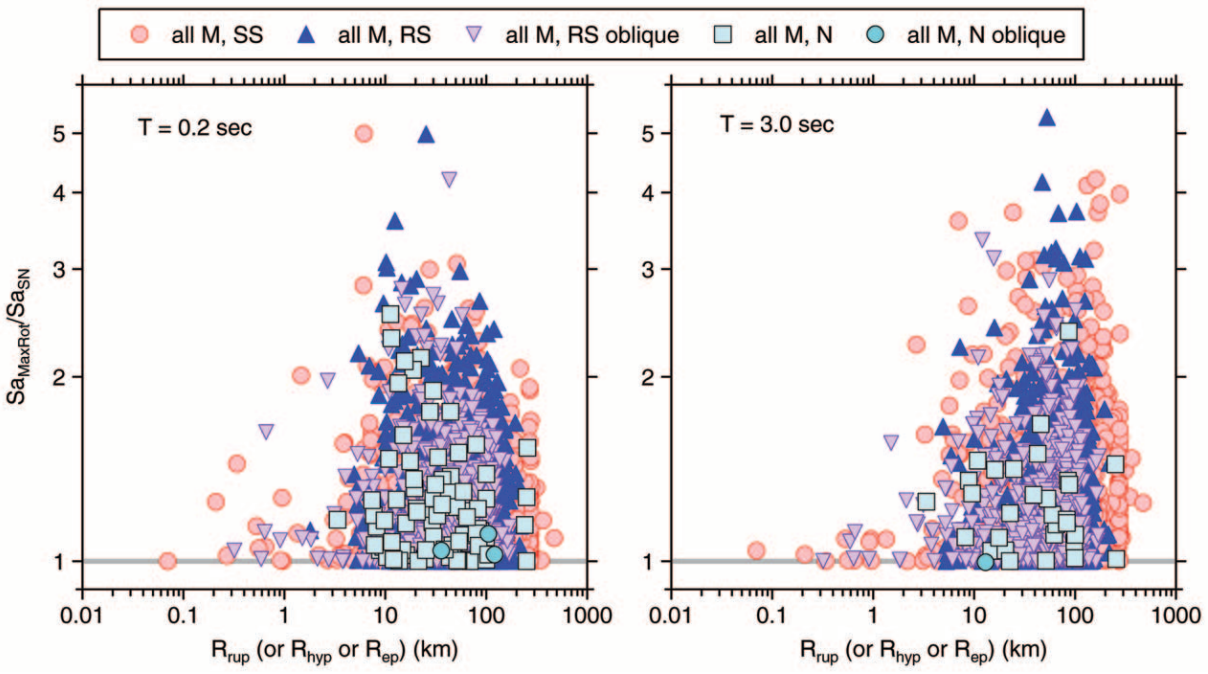

Figure 1. Ratio of Sa_{MaxRot} to Sa_{SN} as a function of closest distance to fault (where available, otherwise hypocentral or epicentral distance, in that order), for all fault types, for oscillator periods of 0.2 and 3.0 sec.

Table 1

Standard Deviation Due to Component-to-Component Variation to Be Used in Adjusting the Aleatory Sigma for Predictions of Sa_{GMRotI} to that of Sa_{Arb} (the Values Are for the Natural Logarithm of Ground Motion)

T (sec)	σ_C*	σ_C†	σ_C‡	σ_C (Average)
−1 (PGV)	0.19	0.207	0.19	0.20
0.0 (PGA)	0.166	0.161	0.166	0.16
0.05	0.162	0.161	0.162	0.16
0.1	0.17	0.161	0.17	0.17
0.2	0.186	0.177	0.186	0.18
0.3	0.196	0.199	0.198	0.20
0.5	0.204	0.227	0.204	0.21
1	0.221	0.253	0.225	0.23
2	0.225	0.253	0.226	0.23
3	0.226	0.253	0.229	0.24
4	0.236	0.253	0.237	0.24
5	0.234	0.253	0.237	0.24

*Data from Boore and Atkinson (2006).
†Data from Beyer and Bommer (2006).
‡Data from Campbell and Bozorgnia (2006).

Crucial to the empirical analysis of Somerville *et al.* is their assumption that directivity amplification causes strong-motion records to have maximum and minimum *Sa* values in the strike-normal and strike-parallel directions. Accordingly, their database consists of strong-motion records rotated to SN and SP directions, and the accuracy of their Sa_{SN} prediction model depends on whether the maximum spectral value is aligned reliably with SN orientations.

Howard *et al.* (2005) evaluated the difference between the direction giving Sa_{MaxRot} and the SN direction, and then the difference between spectral amplitudes of Sa_{MaxRot} and the corresponding predictions of Sa_{SN} at $T = 0.6$, 0.75, 1.0, 1.5, 2.0, and 3.0 sec for each recording station. They found that for reverse-faulting records the misalignment of the direction of Sa_{MaxRot} and the SN direction is up to 76° with an average difference of 29°. They found that the average difference between the orientation of Sa_{MaxRot} and the SN direction for strike-slip records is 21°.

Thus, by limiting an analysis to SN and SP components the engineer is underestimating the magnitude of the largest component. We demonstrate this in Figure 1 by plotting the logarithm of the ratio $Sa_{\mathrm{MaxRot}}/Sa_{\mathrm{SN}}$ (we discuss our algorithm for computing Sa_{MaxRot} in the next section). At distances from the fault less than 3 km and for long periods, $Sa_{\mathrm{MaxRot}}/Sa_{\mathrm{SN}}$ is close to one, but only a few kilometers away it can be as large as a factor of three. For this reason, we provide no adjustment factors for Sa_{SN}, concentrating instead on Sa_{MaxRot}. Before turning to those adjustment factors, however, we investigate Sa_{SN} a bit more to give insight into its dependence on distance and location of the station with respect to the fault.

Figure 2 shows the ratio $Sa_{\mathrm{SN}}/Sa_{\mathrm{SP}}$, with the values for distance less than and greater than 3 km indicated by different symbols. The plot only contains data for strike-slip earthquakes. The ratios are plotted against the angle from the fault to the station, as measured from a point at the middle of the fault. The center of the fault is chosen as the point of reference to provide an average radiation pattern over the entire rupture, not just the radiation from the epicenter, which may

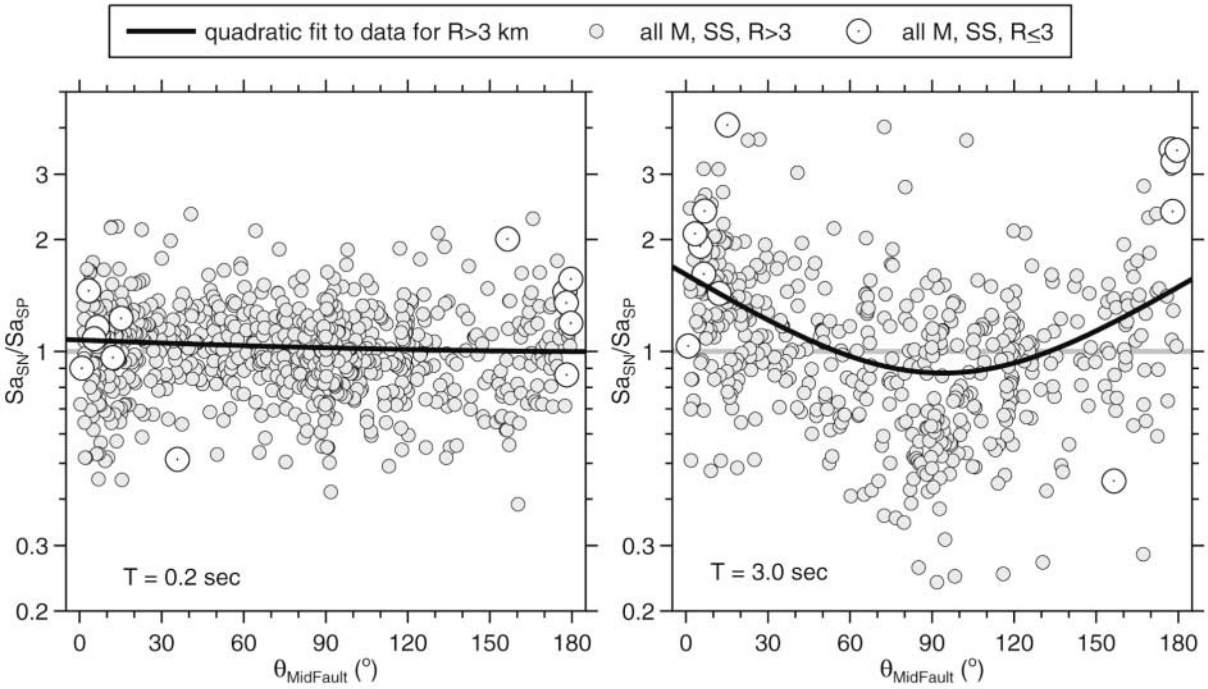

Figure 2. Ratio of Sa_{SN} to Sa_{SP} as a function of the angle between the fault strike and the station, as measured from the midpoint of the fault, for oscillator periods of 0.2 and 3.0 sec. Shown are data only from strike-slip earthquakes. Points within 3 km of the fault are shown by large open circles.

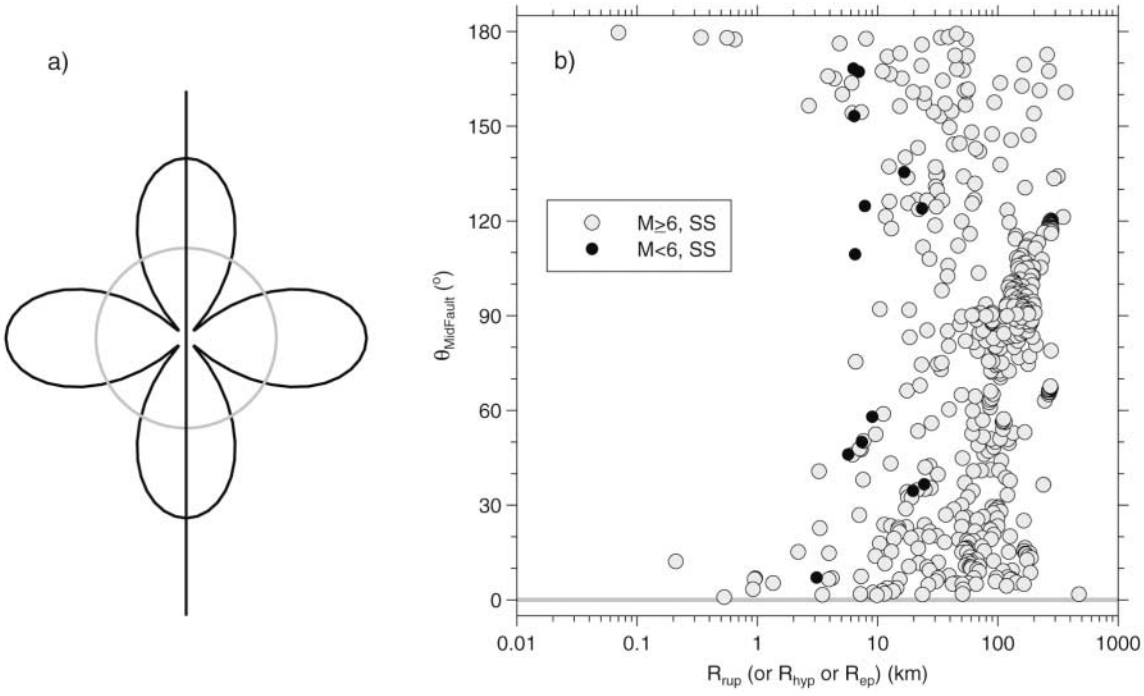

Figure 3. (a) Simplified *SH* wave-radiation pattern, with the gray circle indicating a "water level" of 0.5; the radiation pattern we use in the regression fit consists of the maximum of the water level and $|\cos 2\theta_{\mathrm{MidFault}}|$ for each value of $\theta_{\mathrm{MidFault}}$. The vertical line indicates the fault strike. (b) The distribution of the angle from the station to the midpoint of the fault as a function of distance to the fault for recordings of strike-slip earthquakes.

not be the location from which the majority of the energy is radiated. Except close to the fault, at shorter periods the ratios are almost independent of angle and are distributed almost equally about unity, showing that the strike-normal motion is about equal to the strike-parallel motion on average, independent of station location. For longer periods, however, the ratio clearly depends on station location, with stations located close to the fault and off the ends of the fault having larger strike-normal than strike-parallel motions (we only show results for a period of 3 sec, but we have confirmed our statement for periods out to 5 sec; see also Campbell and Bozorgnia [1994] for a similar observation using data from the 1992 Landers, California, earthquake). The converse is true for stations located roughly perpendicular to the fault, where the strike-parallel motion dominates.

The dominance of Sa_{SN} close to the fault and Sa_{SP} at locations approximately perpendicular to the fault is explicable in terms of the radiation pattern from a vertical strike-slip fault, for which the dominant shear wave should be the *SH* wave, whose motion is transverse to the ray path. Figure 3 shows the radiation pattern for a strike-slip earthquake and rotation angles from the fault to a station as a function of distance for the dataset. Close to the fault we note that the radiation pattern is at a maximum for *SH*-wave radiation, which explains the correlation between Sa_{MaxRot} and Sa_{SN} close to the fault. Figure 4 plots the rotation angle corresponding to Sa_{MaxRot} (the angle is relative to the direction of fault strike and is done separately for each period) against the angle from the fault to the station. Clearly, the rotation angle is near 90° for $T = 3$ sec, which corresponds to the *SH* wave (in a direction normal to the fault strike), for stations located near the fault and off the ends of the fault ($\theta_{MidFault}$ near 0°). For stations at locations nearly perpendicular to the fault ($\theta_{MidFault}$ near 90°), the rotation angles are close to 0 and 180°, which again corresponds to *SH* motion, but now in a strike-parallel direction. This effect was demonstrated by Shakal *et al.* (2006) for ground motions from the 2004 Parkfield, California, earthquake.

A more detailed study of the ratio Sa_{SN}/Sa_{SP} is contained in Spudich and Chiou (2006). They investigated how well the observed ratios were predicted from the radiation patterns expected for the faulting mechanism for each earthquake. Their predicted radiation patterns were an average of the radiation patterns from two locations on the fault. They found that, in general, the radiation pattern becomes more obvious with increasing oscillator period and with decreasing distance to the fault. Our results shown in Figures 2 and 4 are consistent with their more detailed analysis.

Sa_{MaxRot}

As we just showed, the strike-normal component of motion rarely corresponds to the maximum possible response-

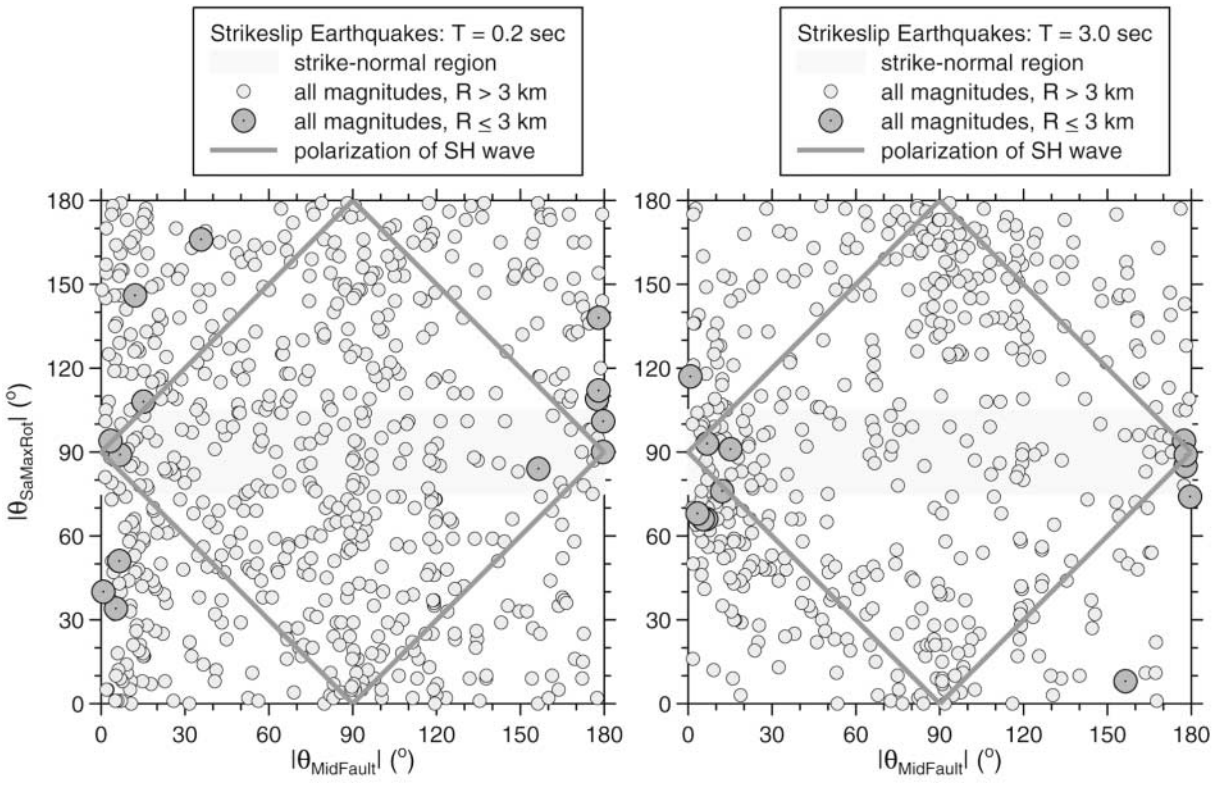

Figure 4. Angles corresponding to Sa_{MaxRot} plotted against the angle between the fault strike and the station, as measured from the midpoint of the fault, for oscillator periods of 0.2 and 3.0 sec. Shown are data only from strike-slip earthquakes. The heavy lines indicate the rotation angle expected for *SH* waves.

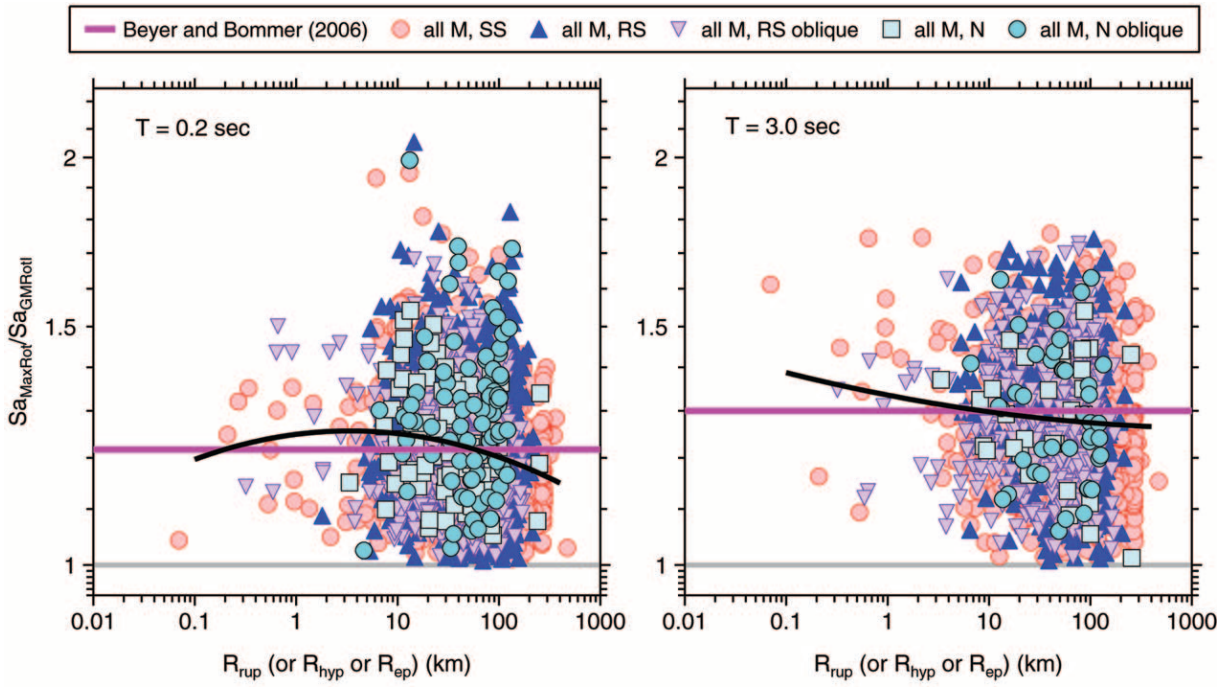

Figure 5. Ratio of Sa_{MaxRot} to Sa_{GMRotI} as a function of closest distance to fault (where available, otherwise hypocentral or epicentral distance), for all fault types, for oscillator periods of 0.2 and 3.0 sec. The black lines show the fit of a quadratic to all of the data, irrespective of mechanism, and are intended only to indicate trends that might otherwise be lost in the large scatter of the data.

spectral measure of seismic ground-motion intensity at a single location. For this reason, we present in this section conversion factors from Sa_{GMRotI} to Sa_{MaxRot}. We compute Sa_{MaxRot} by resolving the two orthogonal components into a direction given by a rotation angle, computing the response spectrum, incrementing the rotation angle, and repeating the process. Sa_{MaxRot} is the maximum value of the response spectrum over all rotation angles. The rotation angle giving the maximum value is period dependent.

We calculate the ratio of $\ln(Sa_{\mathrm{MaxRot}}/Sa_{\mathrm{GMRotI}})$ for the dataset and present the results in Table 2, along with those of Beyer and Bommer (2006). We show plots of $\ln(Sa_{\mathrm{MaxRot}}/Sa_{\mathrm{GMRotI}})$ as a function of distance and magnitude for all classes of fault mechanism in Figures 5 and 6. Also shown in the figures are the ratios given by Beyer and Bommer (2006), whose results are in good agreement with the observations. This is as expected, because they used a subset of the PEER NGA data, although note that our plot includes all Chi-Chi data whereas they did not include those data. The dependence on R and **M** is slight, except perhaps near the fault for $T = 3$ sec and for strike-slip motions. Beyer and Bommer included no R or **M** dependence in their analysis.

For motions from strike-slip faults we also investigate possible dependence of the ratio on the directivity and on the radiation pattern. For the directivity, we use the parameter $X \cos\theta$, where X is the percent of the fault length between the epicenter and the station, as defined by Somerville *et al.* (1997) and θ is the angle from the propagation direction to the station, computed from the epicenter. For the radiation pattern we use the approximation $\cos(2\theta_{\mathrm{MidFault}})$. Plots of $\ln(Sa_{\mathrm{MaxRot}}/Sa_{\mathrm{GMRotI}})$ against these explanatory variables are shown in Figures 7 and 8. It is clear from those figures that the dependence on both is small, even for longer periods. The primary dependence of the ratio on angle is

Table 2
Estimates of the Ratio $\ln Sa_{\mathrm{MaxRot}}/Sa_{\mathrm{GMRotI}}$ from This Research as well as the Ratio of $\ln Sa_{\mathrm{MaxRot}}/Sa_{\mathrm{GM}}$ from Beyer and Bommer (2006)

Period (sec)	Watson-Lamprey and Boore (2007)		Beyer and Bommer (2006)	
	Ratio (Standard Error)	σ	Ratio	σ
PGA	0.184 (0.002)	0.094	0.182	0.040
0.1	0.178 (0.0015)	0.092	0.182	0.040
0.15	0.187 (0.0016)	0.095	0.182	0.040
0.2	0.196 (0.0017)	0.099	0.197	0.043
0.3	0.212 (0.0017)	0.104	0.216	0.048
0.4	0.219 (0.0018)	0.107	0.230	0.052
0.5	0.225 (0.0018)	0.110	0.241	0.054
0.5	0.225 (0.0018)	0.110	0.259	0.059
1	0.237 (0.0019)	0.110	0.262	0.060
1.5	0.237 (0.0019)	0.110	0.262	0.060
2	0.240 (0.0021)	0.112	0.262	0.060
3	0.247 (0.0024)	0.109	0.262	0.060
4	0.256 (0.0031)	0.113	0.262	0.060
5	0.267 (0.0032)	0.114	0.262	0.060

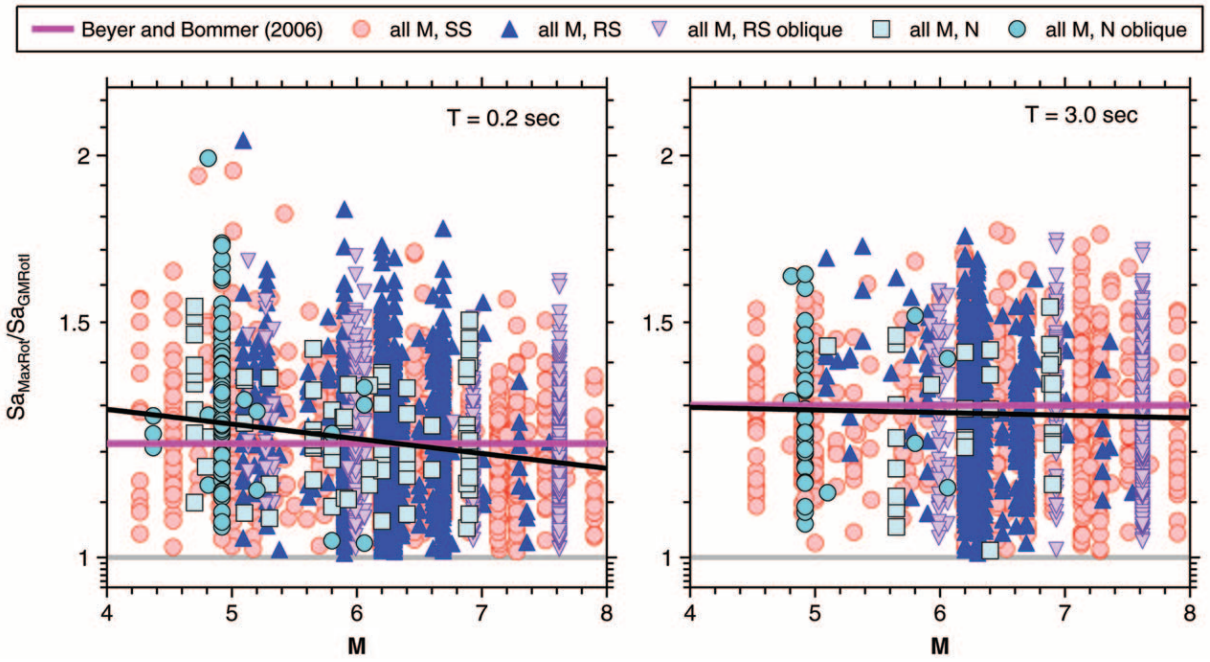

Figure 6. Ratio of Sa_{MaxRot} to Sa_{GMRotI} as a function of moment magnitude for all fault types, for oscillator periods of 0.2 and 3.0 sec. The black lines show the fit of a line to all of the data, irrespective of mechanism, and are intended only to indicate trends that might otherwise be lost in the large scatter of the data.

given by the radiation pattern effect; for this reason we use $\cos(2\theta_{\mathrm{MidFault}})$ as an explanatory variable in the regression equation to be discussed.

Figures 6 through 8 suggest a small or negligible dependence of $\ln(Sa_{\mathrm{MaxRot}}/Sa_{\mathrm{GMRotI}})$ on the explanatory variables. The large scatter in the plots, however, can mask statistically significant dependencies. For this reason we fit $\ln Sa_{\mathrm{MaxRot}}/Sa_{\mathrm{GMRotI}}$ to a function of R, $\mathbf{M}$, and $\theta_{\mathrm{MidFault}}$ using this equation:

$$\ln\left(\frac{Sa_{\mathrm{MaxRot}}(T)}{Sa_{\mathrm{GMRotI}}(T)}\right) = a_1 + a_2\begin{pmatrix} 0 & \text{for } |\cos(2\theta_{\mathrm{MidFault}})| < 0.5 \\ |\cos(2\theta_{\mathrm{MidFault}})| - 0.5 & \text{else}\end{pmatrix} + a_3(M - 6.5) + a_4\begin{pmatrix} 0 & \text{for } R < 15 \\ \ln\dfrac{R}{15} & \text{else}\end{pmatrix} + \sigma \tag{7}$$

The equation was fit using least squares for three cases: (1) strike-slip, normal, and normal-oblique earthquakes with the radiation pattern term; (2) strike-slip, normal, and normal-oblique earthquakes without the radiation pattern term; and (3) reverse and reverse-oblique earthquakes. (Data from strike-slip events dominates cases 1 and 2.) The coefficients were then smoothed. The resulting coefficients for the three cases are given in Tables 3–5 and they are plotted against period in Figure 9 for case 2. The residuals of the data about the regression are plotted against the explanatory variables and X cos θ in Figure 10. Spudich and Chiou (2006) found that for pseudospectral accelerations of 3 sec using X cos θ as a predictor variable decreases standard deviation by 10% and Watson-Lamprey (2007) found a trend in the Abrahamson and Silva (unpublished manuscript, 2007) residuals versus X cos θ with a slope of 0.5. The residuals are not dependent on X cos θ as shown in Figure 10, nor is there any dependence on the explanatory variables. The influence of the large amounts of Chi-Chi data is always a concern. Chi-Chi was a reverse earthquake; thus, these data were not included in cases 1 and 2, but were included in case 3. The coefficients for cases 1 and 2 versus case 3 are not very different, indicating that Chi-Chi has not caused a large impact on the results. The radiation pattern term was found to be small (differences of less than 1% in the prediction of the ratio of Sa_{MaxRot} to Sa_{GMRotI} for all cases except for the predominately strike-slip case.

As a measure of the significance of the results we calculate the fractional reduction in the standard deviation of the regression as compared with the estimates of the ratio $\ln(Sa_{\mathrm{MaxRot}}/Sa_{\mathrm{GMRotI}})$ in Table 2. These fractional reductions are reported in Table 6 for cases 1, 2, and 3. Although the trends calculated versus magnitude and distance are well defined (coefficient standard errors of 15–25%), they do not cause a large change in the standard deviation.

To calculate the correlation coefficient between the ratio of Sa_{MaxRot} to Sa_{GMRotI} and Sa_{GMRotI}, $r_{Y_1,Y_2/Y_1}$, the intraevent residuals from the Abrahamson and Silva (unpublished

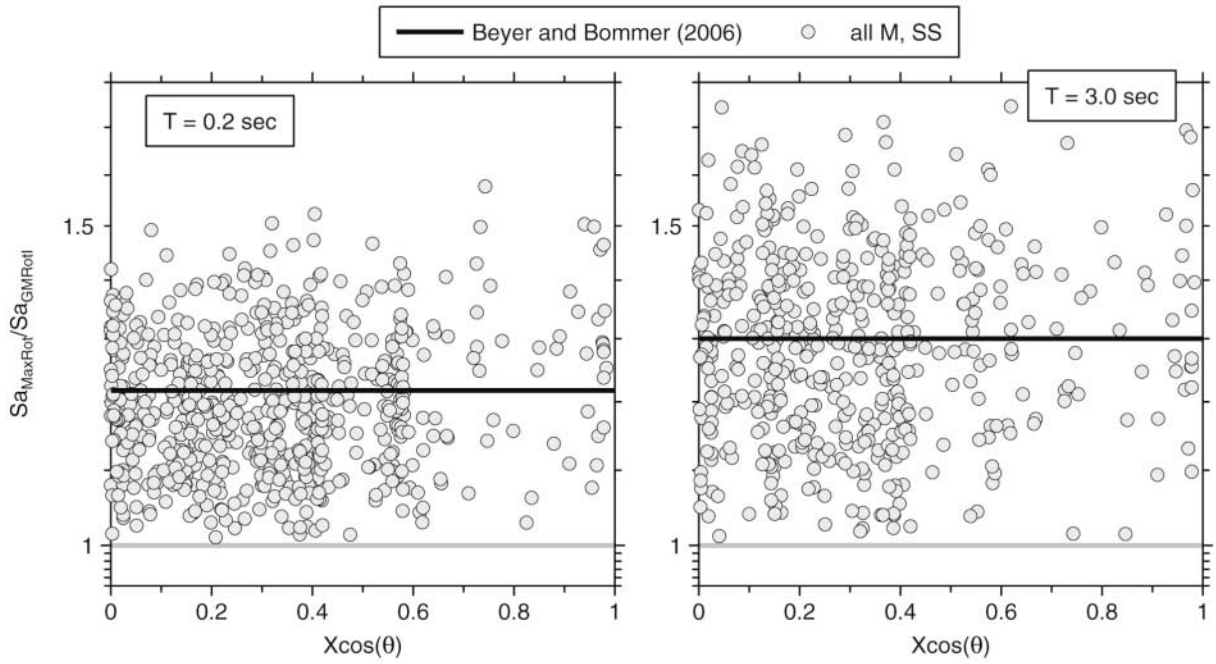

Figure 7. Ratio of Sa_{MaxRot} to Sa_{GMRotI} as a function of the directivity parameter $X\cos(\theta)$ for strike-slip faults, for oscillator periods of 0.2 and 3.0 sec.

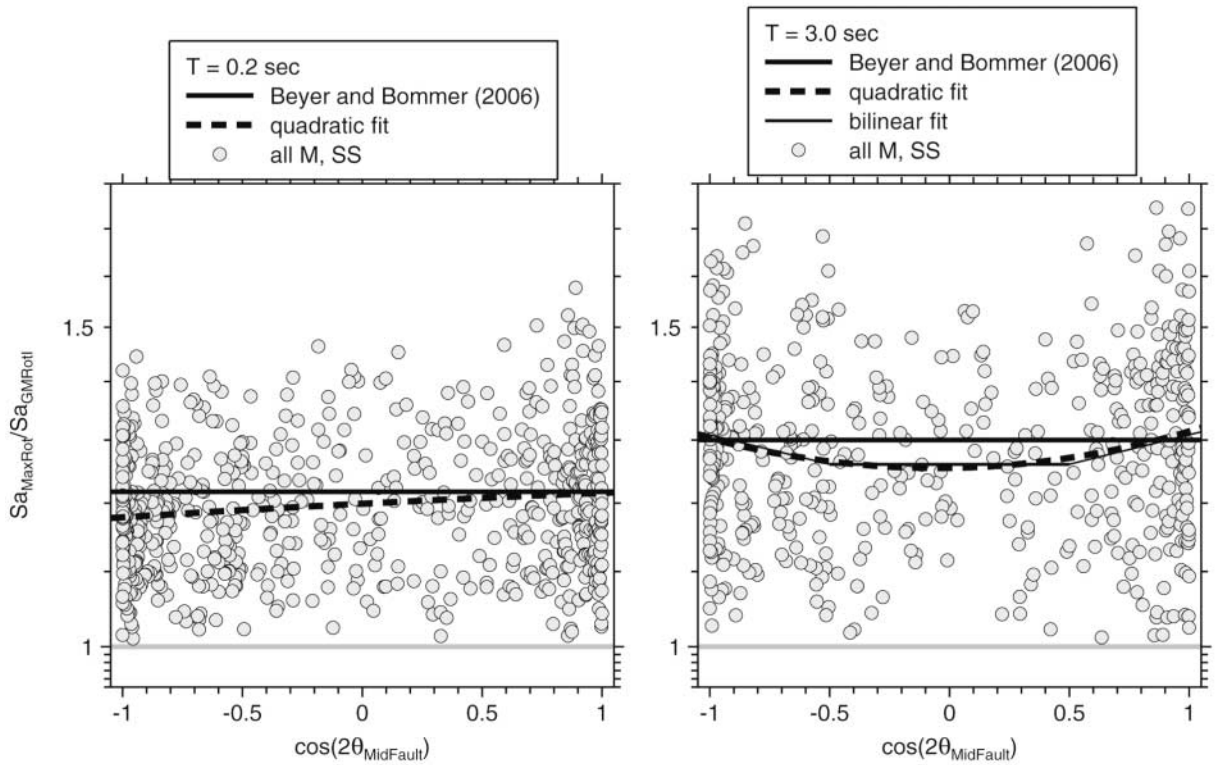

Figure 8. Ratio of Sa_{MaxRot} to Sa_{GMRotI} as a function of the approximate radiation pattern parameter $\cos(2\theta_{\mathrm{MidFault}})$ for strike-slip faults, for oscillator periods of 0.2 and 3.0 sec. The dashed lines show the fit of a quadratic to the data. Note that values of 0.2 and 0.4 for the natural logarithms of the ratios correspond to factors of 1.2 and 1.5 for the ratios, respectively. The thin black line in the right-hand plot shows the fit of a bilinear form to the data (as used in equation 7); it is barely distinguishable from the quadratic fit.

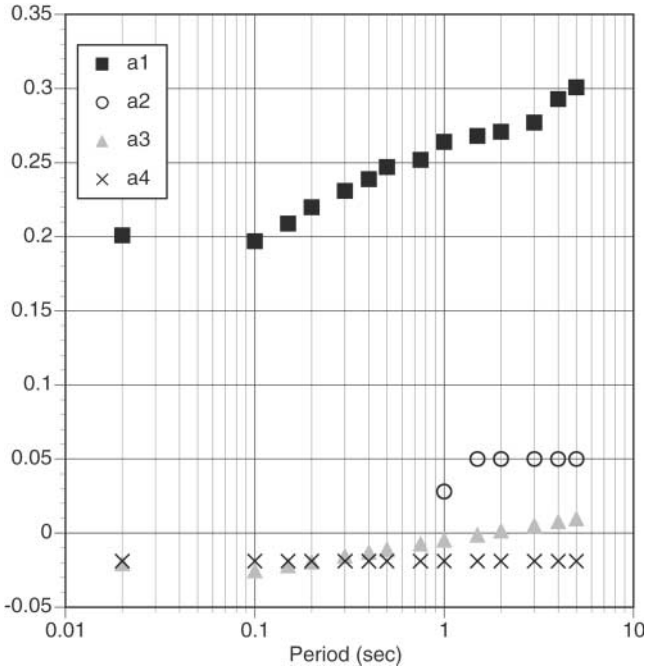

Figure 9. Coefficients of equation (7) relating ln $Sa_{\mathrm{MaxRot}}/Sa_{\mathrm{GMRotI}}$ to various explanatory variables, as a function of oscillator period, for the case when the radiation pattern term is not included. The coefficients are for data from strike-slip earthquakes.

Table 3

Coefficients in Equation for ln $Sa_{\mathrm{MaxRot}}/Sa_{\mathrm{GMRotI}}$ for Strike-Slip, Normal, and Normal-Oblique Earthquakes with the Radiation Pattern Term

T (sec)	a_1	a_2	a_3	a_4	$\sigma_{\ln Sa_{\mathrm{MaxRot}}/Sa_{\mathrm{GMRotI}}}$
PGA	0.201	—	−0.0204	−0.019	0.093
0.1	0.197	—	−0.0253	−0.019	0.092
0.15	0.209	—	−0.0217	−0.019	0.096
0.2	0.220	—	−0.0191	−0.019	0.099
0.3	0.231	—	−0.0154	−0.019	0.099
0.4	0.239	—	−0.0128	−0.019	0.105
0.5	0.247	—	−0.0108	−0.019	0.107
0.75	0.252	—	−0.0072	−0.019	0.108
1	0.264	0.028	−0.0046	−0.019	0.104
1.5	0.268	0.05	−0.001	−0.019	0.104
2	0.271	0.05	0.0016	−0.019	0.112
3	0.277	0.05	0.0053	−0.019	0.116
4	0.293	0.05	0.0079	−0.019	0.114
5	0.301	0.05	0.0099	−0.019	0.118

manuscript, 2007) and Boore and Atkinson (2006) GrMPEs were used with the residuals from equation (7), case 1. The resulting coefficients can be found in Table 7. The parameters have a small correlation (less than 0.18) that approximately decreases with increasing period. There are small differences between the two sets of residuals, but the effect of the correlation is small. Boore *et al.* (2006) show that the orientation of Sa_{GMRotI} is controlled by long-period ground motion. Thus, at long periods Sa_{GMRotI} represents the median

Table 4

Coefficients in Equation for ln $Sa_{\mathrm{MaxRot}}/Sa_{\mathrm{GMRotI}}$ for Strike-Slip, Normal, and Normal-Oblique Earthquakes without the Radiation Pattern Term

T (sec)	a_1	a_2	a_3	a_4	$\sigma_{\ln Sa_{\mathrm{MaxRot}}/Sa_{\mathrm{GMRotI}}}$
PGA	0.201	—	−0.0204	−0.019	0.093
0.1	0.197	—	−0.0253	−0.019	0.092
0.15	0.209	—	−0.0217	−0.019	0.096
0.2	0.220	—	−0.0191	−0.019	0.099
0.3	0.231	—	−0.0154	−0.019	0.099
0.4	0.239	—	−0.0128	−0.019	0.105
0.5	0.247	—	−0.0108	−0.019	0.107
0.75	0.252	—	−0.0072	−0.019	0.108
1	0.264	—	−0.0046	−0.019	0.110
1.5	0.268	—	−0.001	−0.019	0.109
2	0.271	—	0.0016	−0.019	0.111
3	0.277	—	0.0053	−0.019	0.113
4	0.293	—	0.0079	−0.019	0.115
5	0.301	—	0.0099	−0.019	0.116

Table 5

Coefficients in Equation for ln $Sa_{\mathrm{MaxRot}}/Sa_{\mathrm{GMRotI}}$ for Reverse and Reverse-Oblique Earthquakes without the Radiation Pattern Term

T (sec)	a_1	a_2	a_3	a_4	$\sigma_{\ln Sa_{\mathrm{MaxRot}}/Sa_{\mathrm{GMRotI}}}$
PGA	0.207	—	−0.018	−0.019	0.092
0.1	0.201	—	−0.018	−0.019	0.089
0.15	0.209	—	−0.018	−0.019	0.090
0.2	0.217	—	−0.018	−0.019	0.095
0.3	0.236	—	−0.018	−0.019	0.102
0.4	0.243	—	−0.018	−0.019	0.105
0.5	0.249	—	−0.018	−0.019	0.108
0.75	0.256	—	−0.018	−0.019	0.108
1	0.260	—	−0.018	−0.019	0.108
1.5	0.259	—	−0.018	−0.019	0.108
2	0.265	—	−0.018	−0.019	0.111
3	0.276	—	−0.018	−0.019	0.106
4	0.285	—	−0.018	−0.019	0.110
5	0.298	—	−0.018	−0.019	0.110

value of the geometric mean of pseudospectral acceleration. The ratio of Sa_{MaxRot} to Sa_{GMRotI} at long periods is independent of Sa_{GMRotI}. At short periods Sa_{GMRotI} is less likely to be the median value of the geometric mean of pseudospectral acceleration. If Sa_{GMRotI} is high at short periods it may be because Sa_{GMRotI} is above the median value at that period, and vice versa. This would cause a dependence of Sa_{MaxRot} on Sa_{GMRotI} at short periods. The ratio $\ln(Sa_{\mathrm{MaxRot}}/Sa_{\mathrm{GMRotI}})$ is not dependent on amplitude at long periods and is slightly dependent on amplitude at short periods. This dependence is accounted for with a change in standard deviation.

To appreciate better the importance of the magnitude and distance dependence, we show in Figure 11 the conversion factors for a representative set of magnitudes and distances. The figure also shows the individual conversion factors as well as the functional dependence given by Beyer and Bommer (2006). Just looking at the data, our conversion factors are, in general, somewhat smaller than those of Beyer

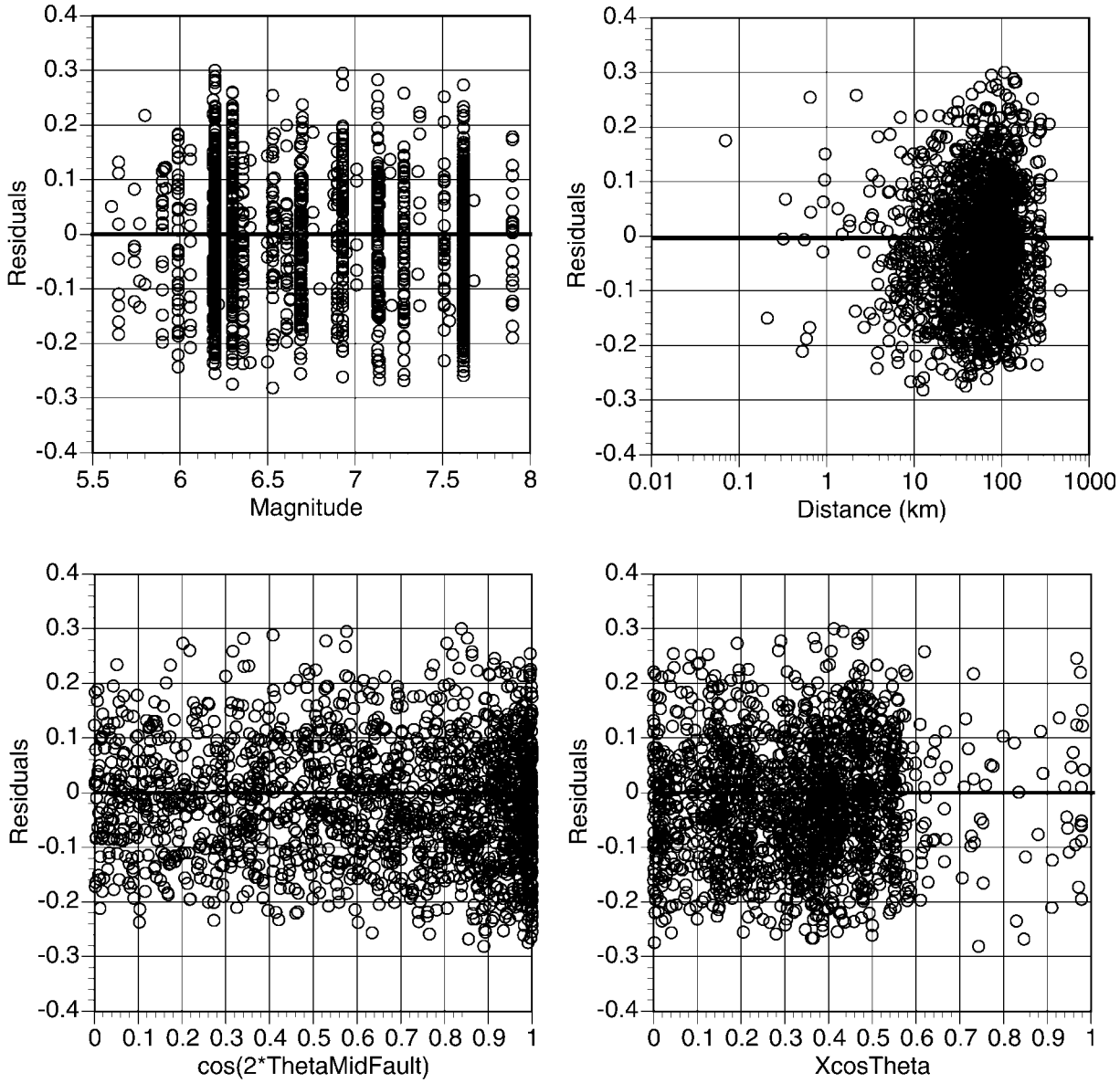

Figure 10. Residuals from equation (7), case 1 for 3-sec pseudospectral acceleration, for all mechanisms.

and Bommer (2006). Both our and their data indicate that the ratio continues to increase with period, unlike their functional form, which has no period dependence above 0.8 sec.

To illustrate the effects of radiation pattern, a plan view of the conversion factors for case 1 for a magnitude 7, strike-slip earthquake are shown in Figure 12. The effect of the shear-wave radiation pattern can be seen, as well as the increase in the ratio of Sa_{MaxRot} to Sa_{GMRotI} near the source. To demonstrate the new median estimates of Sa_{MaxRot} compared with Sa_{GMRotI}, these values are plotted for case 2 for a set of magnitudes versus distance from the rupture in Figure 13.

Equation (7) can be used to convert the values of Sa_{GMRotI} given by GrMPEs to Sa_{MaxRot} by using equations (1) and (2). A complete description of Sa_{MaxRot} also includes the PDF of the quantity. Figure 14 shows the distribution of $\ln(Sa_{\mathrm{MaxRot}}/Sa_{\mathrm{GMRotI}})$ with an approximate fit using a truncated normal distribution. We are not suggesting that Sa_{MaxRot} has a truncated lognormal distribution. Formally, we would have to combine the log-normal distribution of Sa_{GMRotI} with the truncated lognormal distribution of $\ln(Sa_{\mathrm{MaxRot}}/Sa_{\mathrm{GMRotI}})$ to obtain the distribution of Sa_{MaxRot}. The value of $\sigma_{\ln Sa_{\mathrm{MaxRot}}/Sa_{\mathrm{GMRotI}}}$ is much smaller than $\sigma_{\ln Sa_{\mathrm{GMRotI}}}$, however; and thus the error in assuming an untruncated normal distribution for Sa_{MaxRot} with a standard deviation given by $\sigma^2_{\ln Sa_{\mathrm{MaxRot}}} = \sigma^2_{\ln Sa_{\mathrm{GMRotI}}} + \sigma^2_{\ln Sa_{\mathrm{MaxRot}}/Sa_{\mathrm{GMRotI}}}$ is small. As an example of the relative sizes, $\sigma_{\ln Sa_{\mathrm{GMRotI}}}$ for the PEER NGA equations of Boore and

Table 6

Significance of Equation (7) Cases 1, 2, and 3 as Measured by the Fractional Change in Standard Deviation

T (sec)	Case 1	Case 2	Case 3
PGA	−0.043	−0.043	−0.013
0.1	−0.037	−0.037	−0.016
0.15	−0.036	−0.036	−0.024
0.2	−0.041	−0.041	−0.019
0.3	−0.034	−0.034	−0.024
0.4	−0.028	−0.028	−0.022
0.5	−0.034	−0.034	−0.021
0.75	−0.024	−0.024	−0.021
1	−0.017	−0.023	−0.017
1.5	−0.023	−0.020	−0.014
2	−0.052	−0.004	−0.004
3	−0.002	−0.001	−0.005
4	−0.002	−0.005	−0.007
5	−0.003	−0.008	−0.006

Table 7

Correlation Coefficients between the ln Sa_{MaxRot}/Sa_{GMRotI} Residuals of Equation (7), Case 1 and ln Sa_{GMRotI} Residuals from the Abrahamson and Silva (Unpublished Manuscript, 2007) and Boore and Atkinson (2006) GrMPEs

T (sec)	Abrahamson and Silva	Boore and Atkinson
PGA	−0.051	0.089
0.1	0.142	0.148
0.15	0.100	0.168
0.2	0.082	0.123
0.3	0.037	0.047
0.4	0.125	—
0.5	0.020	0.003
0.75	0.041	0.089
1	0.089	0.088
1.5	0.041	−0.011
2	0.089	0.157
3	0.024	−0.005
4	0.046	0.112
5	0.035	0.085

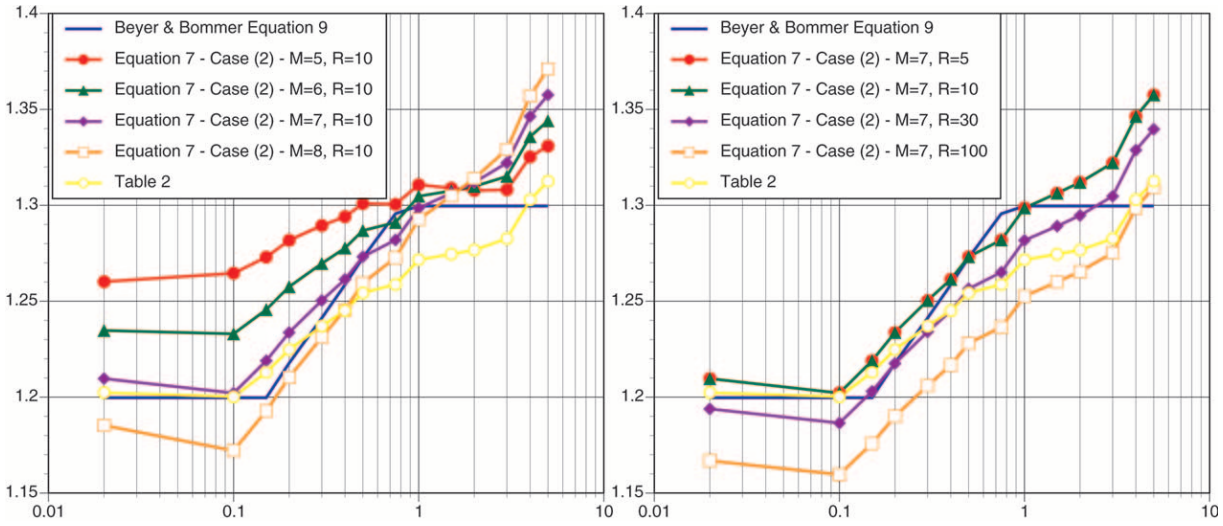

Figure 11. The ratio Sa_{MaxRot}/Sa_{GMRotI} as a function of period for fixed distance and a set of magnitudes (left) and for a fixed magnitude and a set of distances (right). The ratios were determined for case 2: no radiation pattern and predominately strike-slip earthquakes.

Atkinson (2006) is 0.645 for a period of 1 sec. With the $\sigma_{\ln Sa_{MaxRot}/Sa_{GMRotI}}$ of 0.111 for strike-slip earthquakes given in Table 4, and $r_{Y_1,Y_2/Y_1}$ of 0.110 from Table 7, $\sigma_{\ln Sa_{MaxRot}} = 0.666$, which is an incremental contribution to the total aleatory variability of 3%. (In comparison, the conversion from Sa_{GMRotI} to Sa_{Arb} involves a more significant increase in the aleatory variability; from Table 1, we would have $\sigma_{\ln Sa_{Arb}} = 0.688$.)

Conclusions and Discussion

Directivity has become a phenomenon of concern to engineers in recent years because it brought the polarization of ground motion to the awareness of the engineering community. To date, the engineering community has focused solely on the phenomenon in the near-source region and on the strike-normal component of ground motion. We find that focusing on the strike-normal component of ground motion in the near-source region does not capture the maximum possible spectral acceleration over all orientations and underestimates the degree of polarization. We have provided conversion factors from Sa_{GMRotI} to Sa_{MaxRot} which show that the ratio of Sa_{MaxRot} over Sa_{GMRotI} is period dependent, ranging from 1.2 at short periods to 1.35 at long periods. These conversion factors are distance, magnitude, and radiation pattern dependent. The dependencies are small and

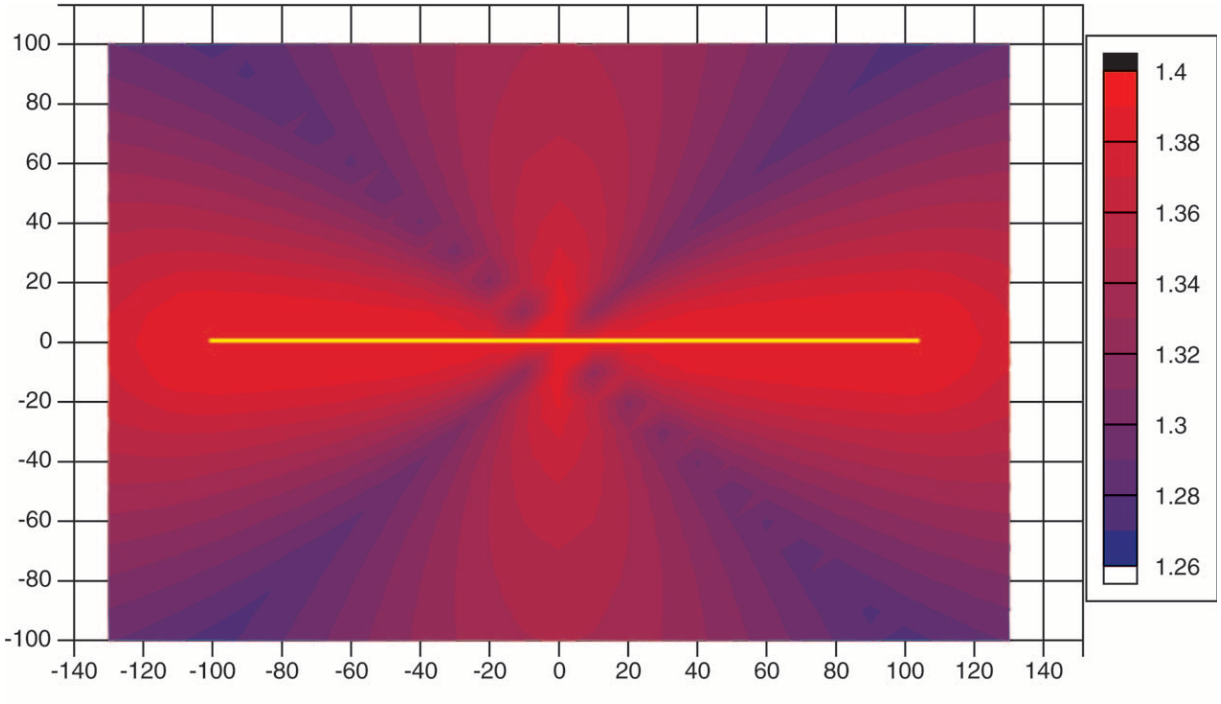

Figure 12. Plan view of the ratio of Sa_{MaxRot} to Sa_{GMRotI} predicted from case 1 for a strike-slip earthquake with a magnitude of 7 at a period of 3 sec. The rupture is shown in yellow; the axes are distances in kilometers.

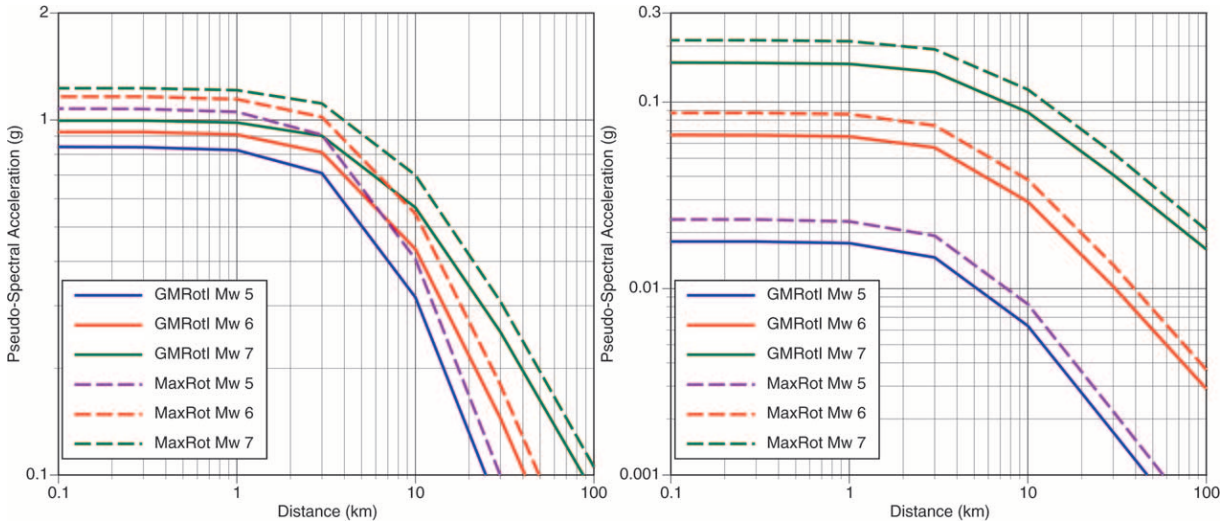

Figure 13. Sa_{MAX} and Sa_{GMRotI}, for case 2: no radiation pattern and predominately strike-slip earthquakes. (a) 0.2-sec pseudospectral acceleration; (b) 3-sec pseudospectral acceleration.

for most engineering applications the conversion factors independent of these variables can be used. Assuming that the ground motion on two orthogonal components peaks at the same time (using the SRSS of the elastic response spectra) slightly overestimates the conversion to maximum spectral acceleration in most cases. We have found that the conversion factors are independent of the most common explanatory variable for directivity. Our results are in broad agreement with those of Beyer and Bommer (2006), who computed constant factors for each period, with no consideration of additional explanatory variables.

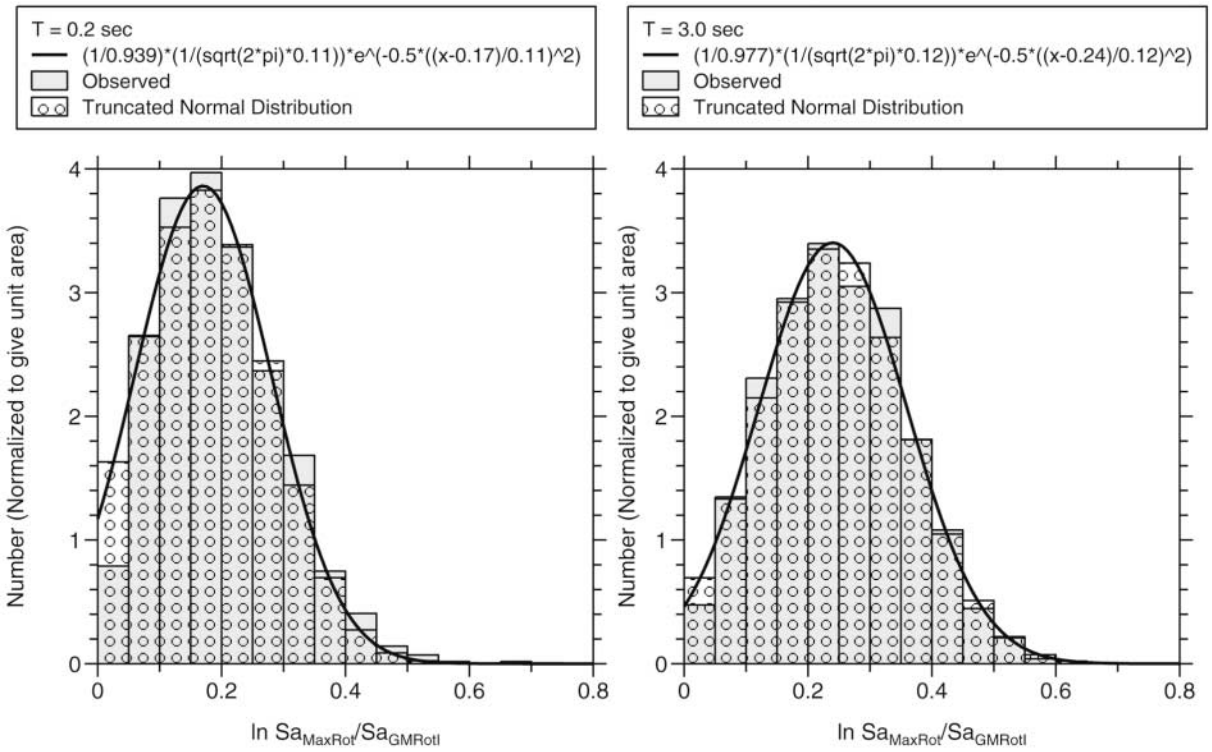

Figure 14. Histograms of the distribution of the observed quantity In $Sa_{\mathrm{MaxRot}}/Sa_{\mathrm{GMRotI}}$ and of the approximate fit to the observed distribution for a truncated normal distribution (given both for the individual bins and for the continuous distribution, with a mean and standard deviation given in the equation shown in the legend).

Acknowledgments

We thank Norm Abrahamson, Jack Baker, Ken Campbell, and Paul Spudich for many stimulating discussions and excellent suggestions.

References

Abrahamson, N. A., and W. J. Silva (1997). Empirical response spectral attenuation relations for shallow crustal earthquakes, *Seism. Res. Lett.* **68,** 94–127.

Baker, J. W., and C. A. Cornell (2006). Which spectral acceleration are you using?, *Earthquake Spectra* **22,** 293–312.

Beyer, K., and J. J. Bommer (2006). Relationships between median values and between aleatory variabilities for different definitions of the horizontal component of motion, *Bull. Seism. Soc. Am.* **96,** 1512–1522.

Boore, D. M. (2005). Erratum to Equations for estimating horizontal response spectra and peak acceleration from western North American earthquakes: a summary of recent work, *Seism. Res. Lett.* **76,** 368–369

Boore, D. M., and G. M. Atkinson (2006). Boore-Atkinson NGA Empirical Ground Motion Model for the Average Horizontal Component of PGA, PGV and SA, PEER Report, http://peer.berkeley.edu/lifelines/nga.html (last accessed January 2007).

Boore, D. M., W. B. Joyner, and T. E. Fumal (1997). , *Seism. Res. Letters* **68,** 128–153.

Boore, D. M., J. Watson-Lamprey, and N. A. Abrahamson (2006). GMRotD and GMRotI: orientation-independent measures of ground motion, *Bull. Seism. Soc. Am.* **96,** 1502–1511.

Campbell, K. W., and Y. Bozorgnia (1994). Empirical analysis of strong ground motion from the 1992 Landers, California, earthquake, *Bull. Seism. Soc. Am.* **84,** 573–588.

Campbell, K. W., and Y. Bozorgnia (2003a). Updated near-source ground motion (attenuation) relations for the horizontal and vertical components of peak ground acceleration and acceleration response spectra, *Bull. Seism. Soc. Am.* **93,** 314–331.

Campbell, K. W., and Y. Bozorgnia (2003b). Erratum to Updated near-source ground motion (attenuation) relations for the horizontal and vertical components of peak ground acceleration and acceleration response spectra, *Bull. Seism. Soc. Am.* **93,** 1413.

Campbell, K. W., and Y. Bozorgnia (2003c). Erratum to Updated near-source ground motion (attenuation) relations for the horizontal and vertical components of peak ground acceleration and acceleration response spectra, *Bull. Seism. Soc. Am.* **93,** 1872.

Campbell, K. W., and Y. Bozorgnia (2004). Erratum to Updated near-source ground motion (attenuation) relations for the horizontal and vertical components of peak ground acceleration and acceleration response spectra, *Bull. Seism. Soc. Am.* **94,** 2417.

Campbell, K. W., and Y. Bozorgnia (2006). Campbell-Bozorgnia NGA empirical ground motion model for the average horizontal component of PGA, PGV, PGD and SA at selected spectral periods ranging from 0.01–10.0 seconds (Version 1.1), PEER-Lifelines Next Generation Attenuation of Ground Motion (NGA) Project, http://peer.berkeley.edu/lifelines/repngamodels.html (last accessed January 2007).

Howard, J. K., C. A. Tracy, and R. G. Burns (2005). Comparing observed and predicted directivity in near-source ground motion, *Earthquake Spectra* **21,** 1063–1092.

Sadigh, K., C.-Y. Chang, J. A. Egan, F. Makdisi, and R. R. Youngs (1997). Attenuation relationships for shallow crustal earthquakes based on California strong motion data, *Seism. Res. Lett.* **68,** 180–189.

Shakal, A., H. Haddadi, V. Graizer, K. Lin, and M. Huang (2006). Some key features of the strong-motion data from the M 6.0 Parkfield, California, earthquake of 28 September 2004, *Bull. Seism. Soc. Am.* **96,** S90–S118.

Somerville, P. G., N. F. Smith, R. W. Graves, and N. A. Abrahamson (1997). Modification of empirical strong ground motion attenuation relations to include the amplitude and duration effects of rupture directivity, *Seism. Res. Lett.* **68,** 199–222.

Spudich, P., and B. S-J. Chiou (2006). Directivity in preliminary NGA residuals, Final Project Report for PEER Lifelines Program Task 1M01, Subagreement SA5146-15811, 49 pp.

Watson-Lamprey, J. A. (2007). The search for directivity, Presented at Seismological Society of America Annual Meeting, 11–13 April 2007, Kona, Hawaii.

Watson-Lamprey Consulting
1212 32nd Street
Oakland, California 94608
Jennie.WatsonLamprey@gmail.com
(J.W.L.)

U.S. Geological Survey, MS 977
345 Middlefield Road
Menlo Park, California 94025
boore@usgs.gov
(D.M.B.)

Manuscript received 9 January 2007.